Molecular Crystals and Liquid Crystals Science and Technology. Section A. Molecular Crystals and Liquid Crystals
Publication details, including instructions for authors and subscription information:
http://www.tandfonline.com/loi/gmcl19

Theory of Pattern Formation in a Freestanding Ferroelectric Film in a Rotating Electric Field

Axel Kilian [a] , H. D. Koswig [b] & André Sonnet [a]
[a] Institut für Theoretische Physik, Technische Universität, Berlin
[b] Ivan-Stranski-Institut Technische Universität, Berlin
Version of record first published: 04 Oct 2006.

To cite this article: Axel Kilian , H. D. Koswig & André Sonnet (1995): Theory of Pattern Formation in a Freestanding Ferroelectric Film in a Rotating Electric Field, Molecular Crystals and Liquid Crystals Science and Technology. Section A. Molecular Crystals and Liquid Crystals, 265:1, 321-334

To link to this article: http://dx.doi.org/10.1080/10587259508041703

Mol. Cryst. Liq. Cryst. 1995, Vol. 265, pp. 321–334
Reprints available directly from the publisher
Photocopying permitted by license only

Theory of Pattern Formation in a Freestanding Ferroelectric Film in a Rotating Electric Field

Axel Kilian†, H. D. Koswig*, and André Sonnet†
†: Institut für Theoretische Physik
*: Ivan-Stranski-Institut
Technische Universität Berlin

1 Abstract

A free-standing ferroelectric film subjected to a rotating electric in-plane field has previously been investigated under a polarizing microscope [1]. Depending on the strength and rotation frequency of the external field, various kinds of pattern formation were observed, e.g. ring systems which can shrink or grow.

This contribution provides a theoretical examination of the effect. It is based on the usual Landau theory [2]. In particular, it is shown that the ring systems observed can be described as inversion walls, which exhibit soliton-like behavior[1]. The analytical results are supported by numerical simulations.

As a result, a qualitative and, to some extend, also a quantitative understanding of the complex behavior of ferroelectric liquid crystals in the case of *inhomogeneously aligned smectic layers* has been achieved.

2 Theory

The phase transition from SmA to SmC^* is accompanied by a symmetry breaking from the higher symmetry D_∞ to C_2. From general symmetry considerations it seems appropriate to choose as an order parameter [2]

$$\vec{\xi} = (\vec{n} \cdot \vec{e})\, \vec{n} \times \vec{e}. \qquad \textbf{Eq. 1}$$

As in nematics, $\vec{n}$ denotes the non-degenerate axis of the dielectric permittivity tensor. In contrast to the axial (unit-) vector $\vec{n}$, $\vec{\xi}$ is a polar vector which lies in the plane of the smectic layers. See Fig. 1.

1. A similar effect in nematics has been reported by Meyer et al. [3].

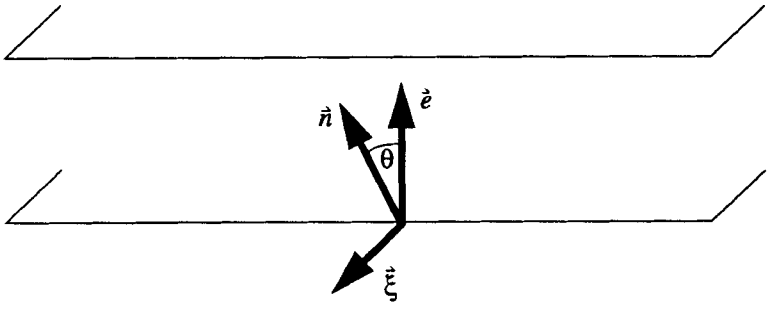

Fig. 1 *A smectic layer.* $\vec{e}$*: layer normal,* $\vec{n}$*: director,* $\vec{\xi}$*:* SmC* *order parameter,* θ*: smectic tilt angle.*

The free energy is

$$F = \int f_{Landau} + f_0 + f_d \, d^3x. \qquad \textbf{Eq. 2}$$

Here, only bulk contributions are taken into account, that is, we neglect possible surface contributions. The Landau energy density is

$$f_{Landau} = a\xi^2 + b\xi^4 + c\xi^6, \qquad \textbf{Eq. 3}$$

where $a = a_o\,(T\text{-}T_{ac})$ is temperature dependency, and a_o, b and c are material coefficients. The next contribution, f_0, contains some invariants built from the order parameter, the spontaneous polarization $\vec{p}_s$, and an electric field $\vec{E}$:

$$f_0 = \mu_p(\vec{p}_s \cdot \vec{\xi}) + \frac{1}{2\varepsilon_\perp} p_s^2 - (\vec{p}_s \cdot \vec{E}) - \frac{\Delta\varepsilon}{2}(\vec{E} \cdot \vec{n}(\vec{\xi}))^2; \qquad \textbf{Eq. 4}$$

μ_p is the piezoelectric coefficient, $\varepsilon_\perp$ the dielectric susceptibility perpendicular to n, $\Delta\varepsilon$ the dielectric anisotropy. The distortion energy is

$$f_d = Kt_o(\vec{\xi} \cdot rot\vec{\xi}) + \frac{K}{2}(\nabla\vec{\xi})^2 + \mu_f(\vec{p}_s \cdot rot\vec{\xi})$$

chiral term (Lifshitz invariant) — elastic energy — flexoelectric contribution

Eq. 5

Here, t_0 is the magnitude of the helical wave vector, i.e. $t_0 = 2\pi / p_0$, p_0 being the pitch; K is an elastic constant. Occasionally, K_3 is written instead of K. This holds when there is no disorder within the smectic layers; then, the smectic order parameter forms a helix, which corresponds to a bend distortion of the director field. Since we consider pattern formation, we prefer to look at K as some effective elastic constant. Finally, μ_f is the flexoelectric coefficient.

A dynamic equation can be obtained using the variational derivative

$$\gamma_1 \frac{\partial \vec{\xi}}{\partial t} = -\frac{\delta F}{\delta \vec{\xi}}. \qquad \textbf{Eq. 6}$$

Here, γ_1 is the rotational viscosity of the ferroelectric liquid crystal. Minimizing Eq. 2 with respect to $\vec{p}_s$ yields

$$\vec{p}_s = -\mu_o \varepsilon_\perp \vec{\xi}, \qquad \textbf{Eq. 7}$$

provided that no electric field is applied and the flexoelectric contribution in Eq. 5 is small (which is usually the case). It seems to be reasonable to assume (and we will do so below) that $\vec{p}_s$ is generally parallel to $\vec{\xi}$ because (from a microscopic point of view) the permanent dipole should somehow be attached to the molecule.

3 Basic Equations

In order to find out which of the various energy contributions are essential for the effect, we start from the following minimum set:

$$f_{Landau}^{simple} = a\xi^2 + b\xi^4 = \frac{A}{2}\xi^2\left(\frac{1}{2}\xi^2 - \xi_{eq}^2\right), \qquad \textbf{Eq. 8}$$

where f_{Landau}^{simple} is a simplified version of Eq. 3, which no longer allows for first-order[1] phase transitions. The material coefficients a and b have been replaced by A = 4b and $\xi_{eq} = \sqrt{-a/2b}$. Likewise, we reduce f_0 (Eq. 4) and f_d (Eq. 5) to

$$f_{elastic} = \frac{K}{2}\left(\nabla \vec{\xi}\right)^2 \text{ and} \qquad \textbf{Eq. 9}$$

$$f_{field} = -\left(\vec{p}_s \cdot \vec{E}\right). \qquad \textbf{Eq. 10}$$

The corresponding dynamic equation is

$$\gamma_1 \frac{\partial \vec{\xi}}{\partial t} = K\nabla^2 \vec{\xi} + W\vec{\xi} + A\vec{\xi}\left(\xi_{eq}^2 - \xi^2\right). \qquad \textbf{Eq. 11}$$

A is the strength of the simplified Landau potential, and $W = |\vec{E}| \cdot |\vec{p}_s|$. For the electric field term, $\vec{p}_s \parallel \vec{\xi}$ has been assumed. As a first approximation, the chiral term is neglected, that is, we assume that the film thickness $d << p_0$. Accordingly, the calculations are essentially 2-dimensional. Later, in chapter 4.3, the effect of the finite pitch is estimated.

The ferroelectric order parameter and the external electric field are parametrized in polar coordinates:

---

1. Such phase transitions occur hardly ever, some have been observed by Heppke et al., cf. [4].

$$\vec{\xi} = S\begin{pmatrix}\sin\varphi\\ \cos\varphi\end{pmatrix};\ \vec{E} = E_0\begin{pmatrix}\sin\Omega t\\ \cos\Omega t\end{pmatrix}. \qquad \textbf{Eq. 12}$$

It follows from Eq. 1 that $S = {}^1/_2\sin(2\theta)$, with θ the smectic C tilt angle. The special cases S = const. and φ = const. are usually referred to as Goldstone mode and soft mode [5]. The dynamic equation for φ is obtained as the z-component of the cross product of $\vec{\xi}$ and Eq. 11:

$$\gamma_1\frac{\partial\varphi}{\partial t} = \frac{W}{S}\sin(\Omega t-\varphi) + K\left(\nabla^2\varphi + \frac{2}{S}\left(\frac{\partial\varphi}{\partial x}\frac{\partial S}{\partial x} + \frac{\partial\varphi}{\partial y}\frac{\partial S}{\partial y}\right)\right). \qquad \textbf{Eq. 13}$$

Similarly, the dynamic equation for S results from the respective scalar product:

$$\gamma_1\frac{\partial S}{\partial t} = W\cos(\Omega t-\varphi) + K\left(\nabla^2 S - S\left(\left(\frac{\partial\varphi}{\partial x}\right)^2 + \left(\frac{\partial\varphi}{\partial y}\right)^2\right)\right) + AS(S_{eq}^2 - S^2). \qquad \textbf{Eq. 14}$$

It is convenient to switch to a coordinate system which rotates with the external field. In terms of the lag angle $\alpha = \Omega t - \varphi$, Eq. 13 and Eq. 14 transform to

$$\gamma_1\frac{\partial\alpha}{\partial t} = \gamma_1\Omega - \frac{W}{S}\sin\alpha + K\left(\nabla^2\alpha + \frac{2}{S}\left(\frac{\partial\alpha}{\partial x}\frac{\partial S}{\partial x} + \frac{\partial\alpha}{\partial y}\frac{\partial S}{\partial y}\right)\right), \text{ and} \qquad \textbf{Eq. 15}$$

$$\gamma_1\frac{\partial S}{\partial t} = W\cos\alpha + K\left(\nabla^2 S - S\left(\left(\frac{\partial\alpha}{\partial x}\right)^2 + \left(\frac{\partial\alpha}{\partial y}\right)^2\right)\right) + AS(S_{eq}^2 - S^2). \qquad \textbf{Eq. 16}$$

We will restrict ourselves to the Goldstone mode. This approximation is valid for moderate electric fields and for temperatures not too close to T_{ac} [5]. As an aside, an equivalent type of simplification is very common in the physics of nematic liquid crystals. It connects the more general alignment tensor theory [6] with the usual director theory.

Thus, only one equation has to be solved, namely

$$\gamma_1\frac{\partial\alpha}{\partial t} = \gamma_1\Omega - W\sin\alpha + K\nabla^2\alpha\ . \qquad \textbf{Eq. 17}$$

In Eq. 17 and below, we have switched from the asymptotic (temperature-independent) material parameters γ_1, K, and $\Delta\varepsilon$ to the actual parameters

$$\gamma_1^{Goldstone} = S_{eq}^2\gamma_1, \qquad \textbf{Eq. 18}$$

$$K^{Goldstone} = S_{eq}^2 K, \text{ and} \qquad \textbf{Eq. 19}$$

$$\Delta\varepsilon^{Goldstone} = S_{eq}\Delta\varepsilon. \qquad \textbf{Eq. 20}$$

From now on, we will sacrifice the superscripts "Goldstone" for brevity. That is, the material parameters K, $\Delta\varepsilon$, and γ_1 that occur below depend on S_{eq} (and therefore on the temperature). Since the tilt angle θ is usually small (typically $< 20^0$), we have

$$S_{eq} = \frac{1}{2}\sin(2\theta) \approx \sin\theta \approx \theta\ , \qquad \textbf{Eq. 21}$$

so that roughly, one can say that $\Delta\varepsilon$ is proportional to θ, whereas K and γ_1 are proportional to θ^2.

4 Analytical Considerations

It is obvious that not much can be done analytically. Even in its simplest form, i.e. specialized to rotational symmetry, Eq. 17 is similar to, but still a little bit more complicated than the overdamped sine-Gordon equation

$$\frac{\partial\Phi}{\partial t} = -\sin\Phi + \frac{\partial^2\Phi}{\partial x^2}, \qquad \textbf{Eq. 22}$$

which has no analytical solutions [8]. It has been studied experimentally because of its soliton-like solutions and its similarity to the original sine-Gordon equation[1], which is a strict soliton equation with well-known analytical solutions [9].

Since our dynamic Eq. 17 is very similar to the soliton Eq. 22, we were not surprised to find also soliton-like solutions, which we present below in chapter 4.2. The soliton-like behavior of the ring systems has meanwhile been supported by recent experiments [10]. As was found, the area of an expanding ring stays constant, when the control parameters are adjusted such that the system is stationary. Provided that the energy density in a ring stays constant during its growth, this means that the total energy is conserved, which is one of the features that characterize solitons.

Actually, this is not the first time that solitons in ferroelectrics are assumed. MacLennan et al. have already described solitary waves which propagate in direction of the layer normal [11].

4.1 Homogeneous Alignment

Homogeneous alignment cannot explain the pattern formation, but it can provide a flavor of what is actually happening in a small region of the liquid crystal. For homogeneous alignment, Eq. 17 simplifies to

$$\tau\frac{\partial\alpha}{\partial t} = \Omega\tau - \sin\alpha. \qquad \textbf{Eq. 23}$$

The dimensionless form has been obtained by defining the system specific time

$$\tau = \frac{\gamma_1}{|\vec{E}| \cdot |\vec{p}_s|}. \qquad \textbf{Eq. 24}$$

Depending on the value of $\Omega\tau$, Eq. 23 has two solutions:

1: $\Omega\tau < 1$,

1. Upon replacing the first derivative in Eq. 22 by a second derivative one obtains the sine-Gordon equation

$$\alpha = \operatorname{asin}(\Omega\tau). \qquad \textbf{Eq. 25}$$

Here, the ferroelectric director follows the applied field synchronously, with a constant lag angle $\alpha < \pi/2$.

2: $\Omega\tau > 1$:

$$\alpha(t) = 2\operatorname{atan}\left[\frac{\omega}{\Omega}\tan\{\frac{\omega}{2}(t - t_{int})\}\right], \text{ where } \omega = \frac{1}{\tau}\sqrt{(\Omega\tau)^2 - 1}, \qquad \textbf{Eq. 26}$$

and t_{int} is an integration constant. Here, the lag angle increases periodically with a "production rate" ω. Every $T = 2\pi/\omega$, α grows by 2π. Note that the threshold $\Omega\tau$ and the production rate ω can be controlled independently via the strength and frequency of the external field. The value $\Omega\tau = 1$ defines the border between both regimes, and it follows that

$$E^{thin}_{\text{sync/async}} = \frac{\Omega\gamma_1}{|p_s|} \qquad \textbf{Eq. 27}$$

This threshold is significant for the pattern formation in thin films, because only in the asynchronous regime, pattern formation can occur. An enhanced formula for films of arbitrary thickness will be given in chapter 4.3.

4.2 Velocity of the Ring Growth

It is known from experiment that the pattern formation is usually more or less spherically symmetric. Assuming that α depends only on the radius r, Eq. 17 simplifies to

$$\zeta_{el}^2(\alpha'' + \frac{1}{r}\alpha') = \tau\dot{\alpha} + \sin\alpha - \Omega\tau. \qquad \textbf{Eq. 28}$$

The primes denotes the derivatives with respect to r, and the electric coherence length

$$\zeta_{el} = \sqrt{\frac{K}{|\vec{E}| \cdot |\vec{p}_s|}} \qquad \textbf{Eq. 29}$$

has been introduced. We look for a travelling-wave solution, i.e. $\alpha(u) := \alpha(r\text{-}vt)$, which yields

$$\zeta_{el}^2(\alpha'' + \frac{1}{r}\alpha') = -v\tau\alpha' + \sin\alpha - \Omega\tau. \qquad \textbf{Eq. 30}$$

For the subsequent estimation of the phase velocity of the wave we neglect the $1/r$ term, i.e. the calculations are valid for rings which are "large enough". This leads to

$$\zeta_{el}^2\alpha'' = -v\tau\alpha' + \sin\alpha - \Omega\tau \qquad \textbf{Eq. 31}$$

Numerical solutions of Eq. 30 and Eq. 31, which have been obtained using the Runge-Kutta algorithm are depicted in Fig. 2. One sees that the travelling-wave solutions for α are 2π inversion walls.

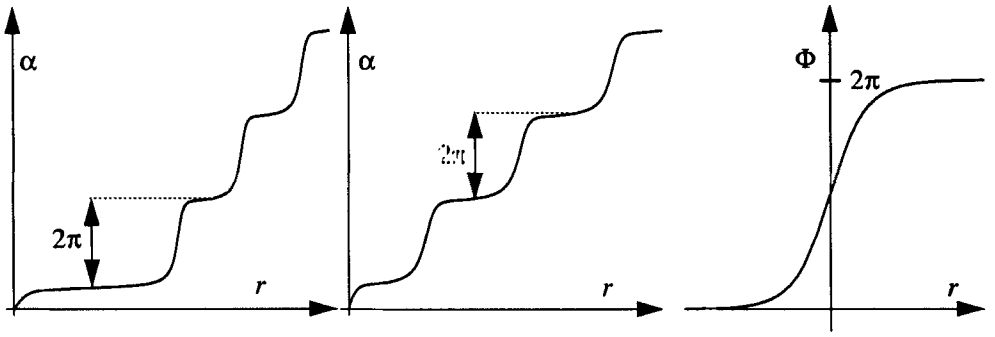

Fig. 2 *Left: numerical solution of Eq. 30. Center: numerical solution of Eq. 31. Right: kink solution of the sine-Gordon equation, cf. Eq. 22.*

Fig. 2a shows a solution of Eq. 30, which differs from Fig. 2b by a larger center region. This is more realistic than Fig. 2b, because the latter solution has been obtained with

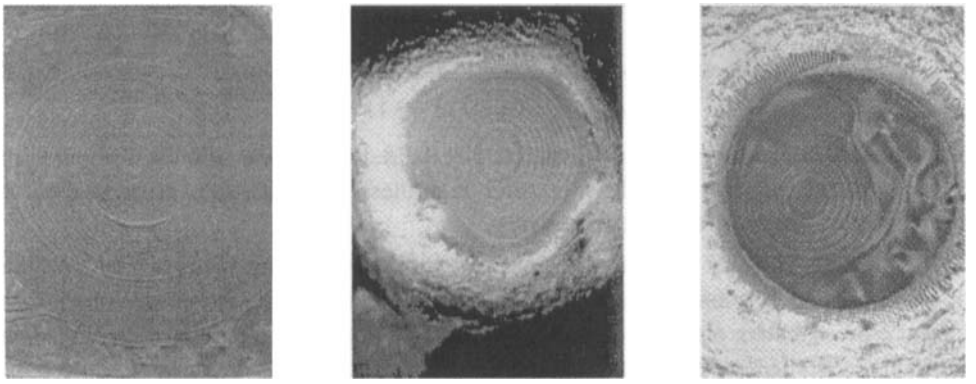

Fig. 3 *Three examples of ring patterns.*

omission of the $1/r$ term. Also, it coincides with experiment, where the nucleation center of a stationary expanding ring system is usually larger then the distance between two rings. See Fig. 3.

By assuming a travelling-wave solution, an artificial control parameter v (the phase velocity) has been introduced. It is aim of this chapter to estimate v. An argument is found by re-interpreting Eq. 31 as a dynamic equation of a particle subjected to an external force $f = -\nabla U$, where

$$U(\alpha) = -(\Omega\tau\alpha + \cos\alpha)\,. \qquad \textbf{Eq. 32}$$

To make the ring growth quasi-stationary, the "dissipation" v must be adjusted such that the dissipation energy and the potential energy cancel, that is

$$-v\tau \int_{-\pi}^{\pi} \alpha' d\alpha = 2\pi\Omega\tau. \qquad \textbf{Eq. 33}$$

The integral has to be taken over one cycle of α', which is 2π. Since no analytic solution of Eq. 31 is available, we use the kink solution of the sine-Gordon equation, which is

$$\alpha = 4\,\mathrm{atan}\left[\frac{e^{-r/\zeta_{el}}}{\sqrt{1-\hat{v}^2}}\right], \text{ where } \hat{v} = v\frac{\tau}{\zeta_{el}} = \frac{\gamma_1}{\sqrt{EKp_s}}. \qquad \textbf{Eq. 34}$$

This is justified by similarity of the shapes of these two functions, which are depicted in Fig. 2b and Fig. 2c. Inserting Eq. 34 in Eq. 33 yields

$$-v\tau \int_{-\pi}^{\pi} \alpha' d\alpha = \frac{8\hat{v}}{\sqrt{1-\hat{v}^2}} \cdot \tanh\frac{d_{sol}}{2\zeta_{el}\sqrt{1-\hat{v}^2}} = 2\pi\Omega\tau, \qquad \textbf{Eq. 35}$$

where d_{sol} is the spatial cycle of α'. Since the phase velocity v, d_{sol}, and the production rate ω (cf. Eq. 26) are related as $2\pi v = \omega d_{sol}$, and ω is a function only of $\Omega\tau$, Eq. 35 is essentially an equation for $\hat{v}$, namely

$$\frac{8\hat{v}}{\sqrt{1-\hat{v}^2}} \cdot \tanh\frac{\pi\hat{v}}{\sqrt{(1-\hat{v}^2)\,((\Omega\tau)^2-1)}} = 2\pi\Omega\tau. \qquad \textbf{Eq. 36}$$

This result is interesting because it predicts that the reduced phase velocity $\hat{v}$ should only depend on the product $\Omega\tau$. This is valid regardless of a possible error due to the approximated shape of the inversion walls.

This phase velocity can, in principle, be compared to experiment. The problem, however, is, that K is usually unknown[1]. In turn, the structure formation could be used to measure the effective elastic constant K. We have checked that the system specific speed $v_0 = \zeta_{el}/\tau = \sqrt{EKp_s}/\gamma_1$ has the same order of magnitude as the velocity at which a ring expands [1], if one assumes $K = 10^{-11}$N (which is the order of magnitude that occurs in nematics). As an example, for the substance FELIX 001 (Hoechst) which has a spontaneous polarization of 7.5 10^{-5}C/m^2 and a rotational viscosity of 64 10^{-3}Pa s, one gets $v_0 = 0.135$ mm/s, when the applied field strength is $E = 10^5$V/m.

1. it could in principle determined by the effect of the helix unwinding, cf. chapter 4.3

We solved Eq. 36 numerically for $1 < \Omega\tau < 9$ using the software *Mathematica*. The result is shown in Fig. 4.

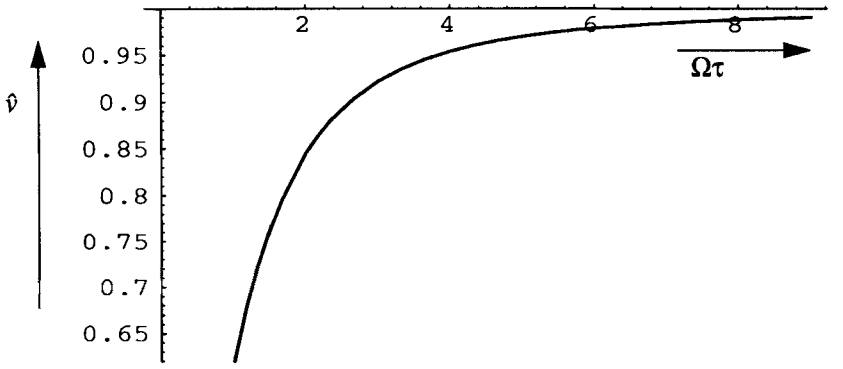

Fig. 4 *Reduced phase velocity of the inversion walls as a function of* $\Omega\tau$, *see Eq. 24.*

It predicts that the phase velocity of the inversion walls depends weakly on $\Omega\tau$, and just above the threshold $E^{thin}_{sync/async}(\Omega\tau=1)$ it should be ~0.65 v_0.

4.3 Effect of the Chirality

So far, chirality has not been taken into account, except in the sense that it is parity breaking and therefore enables the spontaneous polarization. But in films of finite thickness, the direction of the polarization varies over the sample and adds up to a macroscopic polarization which is zero for thick samples ($d >> p_0$). For thin samples with $d < p_o$, the averaged polarization is

$$|\vec{p}_{macro}| = \left|\frac{1}{d}\int_{-d/2}^{d/2}\vec{p}_s dx\right| = |\vec{p}_s|\frac{\sin\pi\hat{d}}{\pi\hat{d}},\ \hat{d} = \frac{d}{p_o}. \qquad \textbf{Eq. 37}$$

This holds when no external field is applied. See Fig. 5. An in-plane electric field unwinds the helix of a sample completely, if it is above a threshold value of

$$E^{inf}_{unwind} = \frac{\pi^2 K t_o^2}{16 p_s}. \qquad \textbf{Eq. 38}$$

Again, $t_0 = 2\pi/p_0$ denotes the magnitude of the helical wave-vector, and the superscript "inf" refers to the fact that Eq. 38 holds only for thick samples with $d \gg p_0$, or samples where the diameter matches exactly the pitch. It has been predicted by R. B. Meyer before ferroelectrics had been available [12]. Unfortunately, his paper contains a printing error, that is, instead of t_0^2, only t_0 occurs. For thin samples ($d < p_0$), the threshold field is given by

$$E_{unwind} = E^{inf}_{unwind}\left[\frac{\pi}{4}\int_0^{d/p_o}\sqrt{2\,(1-\cos\pi x)}\,dx\right]^2 = \hat{E}_{unwind}\frac{\pi^2 K t_o^2}{16 p_s}, \qquad \textbf{Eq. 39}$$

where $\hat{E}_{unwind} = E_{unwind}/E^{inf}_{unwind}$ is depicted in Fig. 5, because no analytic expression is available. The derivation of Eq. 39 can be found in the appendix.

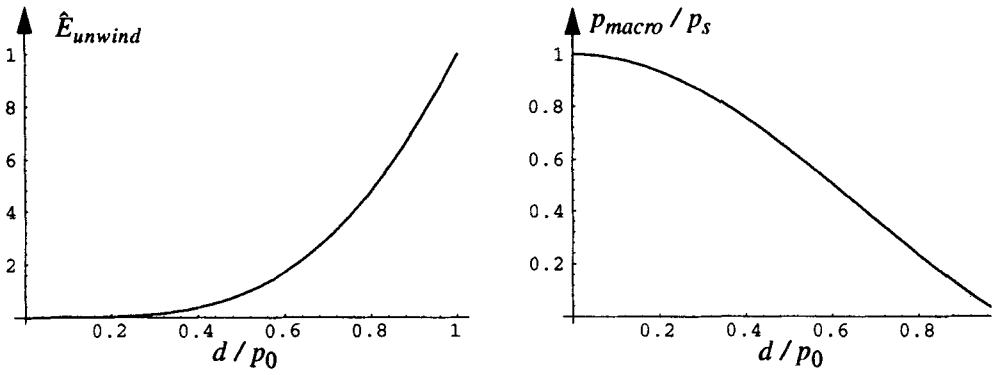

Fig. 5 *Dependence of the critical field for helix unwinding, and of the macroscopic polarization on the reduced cell thickness.*

For the pattern formation, the helical unwinding has the following effect: without helical unwinding, the critical field separating the synchronous from the asynchronous region is proportional to the rotation frequency, see Eq. 27. Since a certain amount of energy is needed to unwind the helix, and the field energy is proportional to the field strength, it should shift the threshold function $E^{thin}_{\text{sync/async}}(\Omega)$ by the field E_{unwind}, i.e.

$$E_{\text{sync/async}} = E^{thin}_{\text{sync/async}} + E_{unwind} = \frac{\Omega\gamma_1}{|p_s|} + \hat{E}_{unwind}\frac{\pi^2 K t_o^2}{16 p_s} . \qquad \textbf{Eq. 40}$$

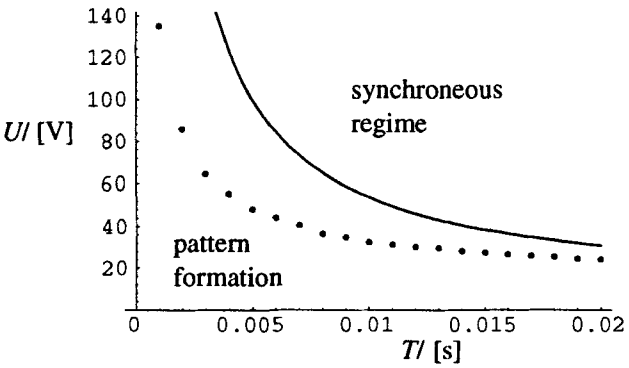

Parameters:

Material:	Mi 15/2 (Halle)
θ:	13.0°
γ_1:	89×10^{-3} mPa s
p_s:	34.7×10^{-5} As/m^2
$d_{Electrode}$:	1.21×10^{-3} m
d_{Layer}:	530×10^{-9} m
p_0:	2.3×10^{-6} m
K:	2×10^{-12} N

Fig. 6 *$E_{sync/async}$ (solid, cf. Eq. 40) compared to experimentally obtained threshold values (dotted) for the pattern formation. The value of K has been assumed to be 2×10^{-12} N, because no measurement data have been available. It is, however, not very critical here.*

In Fig. 6, the theoretically predicted threshold $E_{sync/async}$ is compared to the experimentally obtained one [1]. As can be seen, there is a systematic deviation, which will be discussed in the conclusions.

5 Computer Simulations

One of us (A. Sonnet) has programmed the dynamics according to Eq. 17, using a finite difference scheme. Investigating the dynamic equation with this tool, we learned, that although a travelling-wave solution exists (as was shown in chapter 4.2), nucleation points are necessary to generate the pattern formation. This is the same in experiment, where one or more ring systems can be generated at random sites by dust particles [10]. In the framework of our theoretical model, a nucleation point is a location where the scalar order parameter S is slightly lower than in the environment, and the material parameters are altered according to Eq. 18, Eq. 19, and Eq. 20. This had been done smoothly with Gaussian profiles, and a deviation of 1% was sufficient. We learned that with absolute constant material parameters no nucleation of the inversion walls occurs.

In Fig. 7, a snapshot of a system with two nucleation points is depicted.

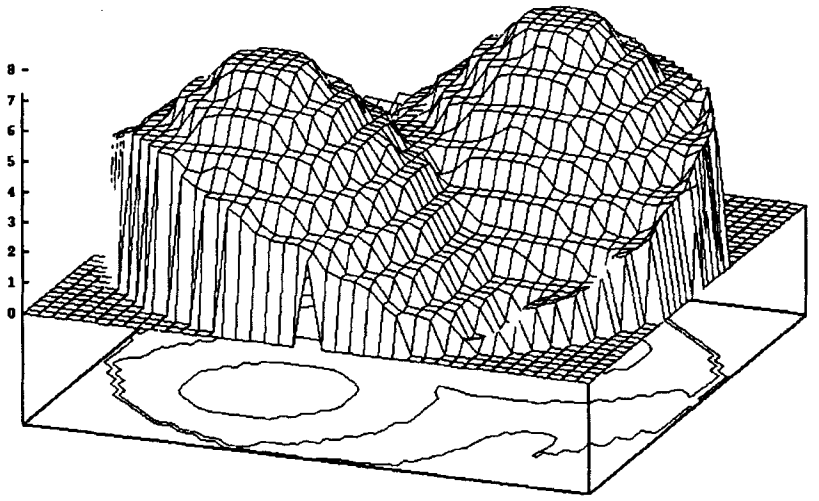

Fig. 7 *Snapshot of the computer simulation of the formation of growing rings. Two nucleation points have been used in order to observe the soliton-like behavior of the inversion walls. The lag angle α between the ferroelectric order parameter and the external field is depicted (in units of 2π).*

6 Conclusions and Acknowledgments

The results of the present paper can be summarized as follows:

1. In principle, the nature of the ring systems that occur in a rotating electric field has been understood. The rings are 2π-inversion walls which propagate soliton-like. The

formation of any ring system requires a nucleation area, where the scalar order parameter is decreased. It consists usually of one or more nucleation points, but it can also be the sample rim that nucleates rings that travel into the center. The reason for the nucleation area to occur can be local homogeneities, impurities, or heating up.

2. The values of the theoretically predicted voltage which separates the synchronous and the asynchronous regimes disagree by a factor up to three from the experimentally found one [10]. The deviations are particularly large at high field strength ($>10^5$ V/m and high frequency >1 kHz). The considerable difference between theoretical and experimental values might have various reasons: firstly, the omission of the dielectric term (cf. Eq. 4), which becomes more efficacious the larger the electric field strength is. Secondly, the heating of the film by dissipation (the power density is $\gamma_1 \Omega^2$). Thirdly, the neglect of possible surface terms, which might be important particularly in thin films.
3. As a new result, the field E_{unwind} which is necessary to unwind the helix of a SmC* film with $d < p_0$ has been calculated. So far, it was known only for $d >> p_0$.

We are indebted to Dr. Hauck for critical discussions and interesting comments.

We thank the Deutsche Forschungsgemeinschaft for financial support via the Sonderforschungsbereich "Anisotrope Fluide".

7 Appendix: Helical Unwinding of a Thin Film

We assume an order parameter field in the Goldstone mode:

$$\vec{\xi} = \begin{bmatrix} \cos(\varphi(z)) \\ \sin(\varphi(z)) \\ 0 \end{bmatrix}. \qquad \textbf{Eq. 41}$$

In contrast to Eq. 12 we use here a unit vector, since the (temperature dependent) material parameters comprise the scalar order parameter S, cf. Eq. 18-Eq. 20. The energy density contains an elastic term, a chiral term, and a field term:

$$f = Kt_o(\vec{\xi} \cdot rot\vec{\xi}) + \frac{K}{2}(\nabla\vec{\xi})^2 - (\vec{p}_s \cdot \vec{E}) \ . \qquad \textbf{Eq. 42}$$

Inserting Eq. 41 in Eq. 42 and dividing by $|\vec{E}| \cdot |\vec{p}_s|$ yields the (dimensionless) energy density

$$\hat{f} = \frac{\zeta^2_{el}}{2}(\varphi'(z))^2 - \zeta^2_{el} t_0 \varphi'(z) - \cos(\varphi) \, . \qquad \textbf{Eq. 43}$$

Again, Eq. 29 has been used. The corresponding Euler-Lagrange equation is

$$\sin(\varphi(z)) - \zeta^2_{el}\varphi''(z) = 0. \qquad \textbf{Eq. 44}$$

After multiplication by $\varphi'(z)$, the first integral is found:

$$\zeta_{el}^2(\varphi'(z))^2 + 2\cos\varphi(z) = C \Leftrightarrow \varphi'(z) = \frac{1}{\zeta_{el}}\sqrt{C - 2\cos\varphi(z)}. \qquad \textbf{Eq. 45}$$

This result, re-inserted in Eq. 43 yields an energy density which contains no more derivatives:

$$\hat{f} = \frac{C}{2} - 2\cos(\varphi(z)) - \zeta_{el} t_o \sqrt{C - 2\cos(\varphi(z))}. \qquad \textbf{Eq. 46}$$

Through the sample, the microscopic polarization rotates by an angle of

$$\psi = 2\pi\frac{d}{p_o}, \qquad \textbf{Eq. 47}$$

when no external field is present. Conversely, the length corresponding to a given rotation angle ψ can be expressed using Eq. 45 as

$$l = 2\int_0^{\psi/2} \frac{\zeta_{el}}{\sqrt{C - 2\cos\varphi}} d\varphi; \qquad \textbf{Eq. 48}$$

At zero field, $l = d$, and l diverges at the critical field to be calculated. The mean energy density is

$$\bar{F} = \frac{1}{l}\int_{-l/2}^{l/2} \hat{f}(z)\,dz = \frac{2}{l}\int_0^{\psi/2} \hat{f}(z) \frac{\zeta_{el}}{\sqrt{C - 2\cos\varphi}} d\varphi = \qquad \textbf{Eq. 49}$$

$$\frac{2}{l}\int_0^{\psi/2} \left[\frac{1}{2}(C - 2\cos\varphi) + \zeta_{el} t_o \sqrt{C - 2\cos\varphi} - \cos\varphi\right] \frac{\zeta_{el}}{\sqrt{C - 2\cos\varphi}} d\varphi = \qquad \textbf{Eq. 50}$$

$$\frac{2}{l}\int_0^{\psi/2} \sqrt{C - 2\cos\varphi}\, d\varphi - \frac{2\pi\zeta_{el} t_o}{l} - \frac{C}{2}. \qquad \textbf{Eq. 51}$$

Now, $C(E)$ can be determined such that $\bar{F}$ is minimized. The necessary condition is

$$\frac{d\bar{F}}{dC} = \left[-\frac{2}{l^2}\int_0^{\psi/2} \sqrt{C - 2\cos\varphi}\, d\varphi + \frac{2\pi\xi_{el} t_o}{l^2}\right]\frac{dl}{dC} = 0, \text{ or} \qquad \textbf{Eq. 52}$$

$$\pi t_o \sqrt{\frac{K}{|\vec{E}| \cdot |\vec{p}_s|}} = \int_0^{\psi/2} \sqrt{C - 2\cos\varphi}\, d\varphi = I(\psi). \qquad \textbf{Eq. 53}$$

This equation defines a threshold value for E, above which no solution for $C(E)$ exists. The smallest possible value for C is 2, and consequently, the critical field to unwind the helix is

$$E_{unwind} = \frac{\pi^2 K t_o^2}{I^2(\psi)\, p_s}. \qquad \textbf{Eq. 54}$$

Since $\psi = 2\pi$ yields the threshold for thick samples ($d \gg p_0$), and $I(2\pi) = 4$, Eq. 38 and Eq. 39 follow.

8 References

[1] G. Hauck, H. D. Koswig, Ferroelectrics **122**, 253 (1991);
G. Hauck, H. D. Koswig, and U. Labes, Liquid Crystals **14**, 991 (1993);
G. Hauck, H. D. Koswig, and U. Labes, in *Modern Topics in Liquid Crystals*, ed. A. Buka, World Scientific Publishing Singapore (1993)

[2] S. A. Pikin and M. A. Osipov in: *Ferroelectric Liquid Crystals*, ed. G. W. Taylor, Gordon and Breach Science Publishers, Philadelphia (1991)

[3] K. B. Migler and R. B. Meyer, Phys. Rev. Lett. **66**,1485(1991)

[4] Ch. Bahr and G. Heppke, Mol. Cryst. Liq. Cryst. **148**, 29 (1987); 151, **69** (1987)

[5] N. A. Clark and S. T. Lagerwall in: *Ferroelectric Liquid Crystals*, ed. G. W. Taylor, Gordon and Breach Science Publishers, Philadelphia (1991)

[6] S. Hess, Z. Naturforsch. **30a**, 728; 1224 (1975)

[7] Ch. Bahr and D. Fliegner, Phys. Rev. A **46**, 7657 (1992)

[8] J. R. Waldram et al., Philos. Trans. R. Soc. London **268**, 265 (1970)

[9] *Solitons*, ed. R. K. Bullough and P. J. Caundrey, Springer, N.Y. (1980)

[10] G. Hauck and H. D. Koswig, Proc. 15. ILCC

[11] J. E. MacLennan, N. A. Clark, and M. A. Handschy in: *Solitons in Liquid Crystals*, ed. L. Lam and J. Prost, Springer Verlag, N. Y. (1991)

[12] R. B. Meyer, Mol. Cryst. Liq. Cryst. **40**, 33 (1977)